Parameterization of cloud droplet size distributions: comparison with parcel models and observations

W. C. Hsieh[1], H. Jonsson[2], G. Buzorius[3], R. C. Flagan[4,5], J. H. Seinfeld[4,5], and A. Nenes[1,6]

A. Nenes, nenes@eas.gatech.edu

[1]School of Earth and Atmospheric

Abstract. This work examines the efficacy of various physically-based approaches derived from 1-D adiabatic parcel model frameworks (a numerical model and a simplified parameterization) to parameterize the cloud droplet distribution characteristics for computing cloud effective radius and auto-

Sciences, Georgia Institute of Technology, Atlanta, Georgia, USA

[2]Center for Interdisciplinary Remotely-Piloted Aircraft Studies, Naval Postgraduate School, Monterey, California, USA

[3]Naval Postgraduate School, Monterey, California, USA

[4]Environmental Science and Engineering, California Institute of Technology, Pasadena, California, USA

[5]Department of Chemical Engineering, California Institute of Technology, Pasadena, California, USA

[6]School of Chemical and Biomolecular Engineering, Georgia Institute of Technology, Atlanta, Georgia, USA

conversion rate in regional/global atmospheric models. Evaluations are carried out for integrations with single (average) and distributions of updraft velocity, assuming that a) conditions at s_{max} are reflective of the cloud column, or, b) cloud properties vary vertically, in agreement with 1-D parcel theory. The predicted droplet distributions are then compared against in-situ cloud droplet observations obtained during the CRYSTAL-FACE and CSTRIPE missions. Good agreement of droplet relative dispersion between parcel model frameworks indicates the parameterized parcel model essentially captures 1-D dynamics; the predicted distributions are overly narrow, with relative dispersion being a factor of 2 lower than observations. However, if conditions at cloud maximum supersaturation are used to predict relative dispersion and applied throughout the cloud column, better agreement is seen with observations, especially if integrations are carried out over the distribution of updraft velocity. When considering the efficiency of the method, calculating cloud droplet spectral dispersion at s_{max} is preferred for linking aerosol with droplet distributions in large scale models.

1. Introduction

The greatest uncertainty in assessments of anthropogenic climate change arises from aerosol-cloud-climate interactions [*Intergovernmental Panel on Climate Change (IPCC)*, 2007], termed "aerosol indirect effects". Increased aerosol concentrations tend to increase the number of droplets in warm clouds, which can enhance cloud albedo [*Twomey*, 1977]; increasing droplet number also tends to reduce precipitation efficiency, which can affect cloud structure, lifetime and radiative properties [*Albrecht*, 1989].

Quantifying indirect effects requires a relationship between cloud microphysical properties (like number and size distribution) and its precursor aerosol. Current treatments range from empirical correlations between an aerosol proxy (such as mass) and a droplet distribution moment (typically number) [*Boucher and Lohmann*, 1995], to explicit calculation of droplet number using a "mechanistic parameterization" [*Ghan et al.*, 1997; *Nenes and Seinfeld*, 2003; *Fountoukis and Nenes*, 2005; *Barahona and Nenes*, 2007]. Although this is an important step towards addressing issues of aerosol-cloud interactions, calculation of droplet number and cloud liquid water content alone are not sufficient. Cloud processes are sufficiently sensitive to droplet size, so parameterizations must also include some measure of the droplet distribution. For example, autoconversion of cloud water to rain (i.e., formation of drizzle from self collision of small droplets) is a key cloud process and very sensitive to droplet size distribution; in fact, the largest uncertainty in assessment of aerosol impacts on precipitation is associated with the treatment of rain formation in large scale models [*Lohmann and Feichter*, 2005]. Although numerous autoconversion parameterizations exist (e.g. *Kessler* [1969]; *Manton and Cotton* [1977]; *Rotstayn* [1997];

Khairoutdinov and Kogan [2000]; *Liu and Daum* [2004], the uncertainty associated with their application is large, about a factor of ten [*Hsieh et al.*, in press], and largely related to the treatment of droplet size distribution and the size-dependence of the collection kernel.

Explicit consideration of droplet size distribution is important also for calculation of cloud radiative properties. The effective radius, required for calculation of cloud optical depth and radiative forcing, is given by $r_e = (\frac{3L}{4\pi\rho_w kN})^{1/3}$, where ρ_w is the density of water, and the spectral parameter "k" expresses the effect of droplet width; k=1 for monodisperse droplets, decreasing as the distribution broadens. For example, *Martin et al.* [1994] proposed k=0.80 for marine clouds (narrow size distribution) and k=0.67 for polluted clouds (broad size distribution). Although qualitatively correct, these k values do not capture the extent of variability in droplet distribution width seen in ambient clouds. *Liu and Daum* [2000, 2002] recognized this and derived formulas for r_e by assuming droplets follow a Weibull or gamma size distribution, and explicitly included the effect of relative dispersion (i.e., the ratio of standard deviation to average radius). When included in GCM assessments of the indirect effect, variability in droplet spectral broadening decreased indirect forcing between 14.3 and 16% [*Peng and Lohmann*, 2003; *Rotstayn and Liu*, 2003], with an upper limit of 33.1% [*Rotstayn and Liu*, 2003].

Understanding the processes that control the width of observed size distributions in ambient clouds has been the focus of many studies in the past. All agree that single updrafts, where droplets grow via condensation, tend to produce narrow size distributions; considering entrainment and mixing can substantially broaden them [*Mason and Chien*, 1962; *Mason and Jonas*, 1974; *Baker et al.*, 1980; *Cooper*, 1989; *Su et al.*, 1998; *Lasher-*

Trapp et al., 2005, e.g.,]. Other processes can broaden the distribution as well, such as collision-coalescence [*Pruppacher and Klett*, 1997, e.g.,], and secondary activation of droplets above cloud base [*Erlick et al.*, 2005].

Although resolving the droplet size distribution is required to reduce the uncertainty of aerosol indirect effects, explicit cloud droplet microphysics is computationally expensive. Parameterizations reduce the computational burden, but may (as seen in the previous examples) introduce significant predictive uncertainty. Efficient parameterization of droplet spectral width and its dependence on the cloud microphysical state (and changes thereof from aerosol perturbations) is an active area of research. *Wood* [2005] proposed a generalized droplet distribution derived from observational data; a number of physically-based alternatives have also been proposed to link aerosol with cloud distribution properties. *Khvorostyanov and Curry* [1999] also relate N and droplet distribution width to cloud parameters such as updraft velocity dispersion and the vertical profile of cloud thermodynamic properties. Similarly, the cloud droplet spectrum tends to broaden when the updraft velocity decreases [*Peng et al.*, 2007; *Yum and Hudson*, 2005]. *Liu et al.* [2006] derived an analytical formula that relates the relative dispersion of cloud droplet distribution to cloud condensation nuclei (CCN) spectra and updraft velocity, based on adiabatic growth theory of cloud droplets. These approaches apply some form of parcel theory towards computing cloud droplet spectral properties. However, few studies exist that evaluate, through the usage of in-situ cloud observations, the uncertainty in predicted droplet spectral parameters and autoconversion associated with application of parcel-based approaches.

In this work, we explore the potential of parcel-based approaches for parameterizing cloud droplet size distribution in regional and global climate models. All approaches tested assume droplets form adiabatically in individual updrafts (using a parcel model and a parameterization thereof based on the *Nenes and Seinfeld* [2003] and *Fountoukis and Nenes* [2005] activation parameterizations) to explicitly compute the size distribution and growth of an activated droplet population throughout a cloud column. We also explore another approach, based on computing the relative dispersion at s_{max} using the *Nenes and Seinfeld* [2003] parameterization, assuming that it applies to the whole cloud column. The overall droplet distribution, $n(D_p)$, is then computed for either a single updraft (corresponding to the average of the measured distribution), or as the superposition of droplet distributions for each updraft measured in the cloud. Each approach is evaluated by comparing predicted droplet spectral characteristics with in-situ measurements of cloud droplet size distributions for a wide range of aerosol and cloud forming conditions sampled during the CRYSTAL-FACE [*Conant et al.*, 2004] and CSTRIPE field compaigns [*Meskhidze et al.*, 2005]. The importance of predicted size distribution deviations is expressed in terms of the uncertainty in the predicted spectral dispersion parameter k, and autoconversion rate; the latter is done by introducing parameterized and observed size distributions into the R_6 (i.e., sixth-moment mean radius) parameterization of *Liu and Daum* [2004], and quantifying the resulting differences in autoconversion.

2. Simulating cloud droplet growth

2.1. Numerical parcel model

Computation of the cloud droplet size distribution is based on the 1-D adiabatic cloud parcel framework, in which buoyant air parcels develop water vapor supersaturation, and

cloud droplets activate upon aerosol particles contained within them. After a maximum supersaturation, s_{max}, is reached, all droplets have formed and grow subsequently via condensation. Since a cloud is characterized by a distribution of updrafts, the parcel concept can be further extended, so that the average droplet number and size distribution is the superposition of distributions from each updraft (or some moment thereof, e.g., *Meskhidze et al.* [2005]; *Peng et al.* [2005]; *Fountoukis et al.* [2007]).

2.2. Parameterization of parcel model

Instead of numerically solving the full set of differential equations that describe the process of activation and condensational growth (e.g., *Nenes et al.* [2001]), we develop a simplified approach that involves two steps: *i*) calculation of the cloud drop number concentration and size distribution at the point of s_{max}, using one of the activation parameterizations of *Nenes and Seinfeld* [2003], *Fountoukis and Nenes* [2005], or *Barahona and Nenes* [2007], and, *ii*) simulation of the subsequent droplet growth as the cloud parcel ascends through a simplified treatment of condensational growth.

2.2.1. Determination of cloud drop size distribution at s_{max}

According to Köhler theory, a cloud condensation nucleus (CCN) requires exposure to a minimum "critical" supersaturation, s_c, before it can experience unconstrained growth and transform into a cloud droplet. s_c depends on particle size and chemical composition; therefore, the number of droplets forming in a cloud can be computed if the cloud supersaturation and the aerosol properties are known. In the initial stages of cloud formation, cooling of the air parcel leads to water vapor supersaturation; CCN then begin to activate into cloud droplets and rapidly grow. When enough CCN activate, the condensation of water vapor is strong enough to balance the availability of water vapor for condensation

(through cooling); this is the point where supersaturation reaches its maximum value, s_{max}, and determines the number of droplets that form [*Nenes et al.*, 2001]. Numerical parcel models simulate this process by solving a system of coupled differential equations (e.g., *Nenes et al.* [2001]), an approach that is computationally too demanding to be included within a global model. Instead, simplified approaches, known as "mechanistic activation parameterizations" [e.g., *Abdul-Razzak et al.*, 1998; *Nenes and Seinfeld*, 2003; *Fountoukis and Nenes*, 2005; *Barahona and Nenes*, 2007] predict CDNC at the point of s_{max} in an ascending parcel; of these, the formulations of *Nenes and Seinfeld* [2003], *Fountoukis and Nenes* [2005] and *Barahona and Nenes* [2007] explicitly predict the droplet size distribution (i.e., the concentration of droplets, dN, within a wet diameter interval dD_p) at s_{max}, as the size of all activated droplets is known. Droplet size is determined from the droplet growth equation, [*Pruppacher and Klett*, 1997; *Seinfeld and Pandis*, 1998],

$$\frac{dD_{pi}}{dt} = \frac{G}{D_{pi}}\left(s - s_{eq}\right) \tag{1}$$

$$G = \frac{4}{\frac{\rho_w RT}{p^s D_v M_w} + \frac{\Delta H_v \rho_w \left(\frac{\Delta H_v M_w}{RT} - 1\right)}{\kappa_a T}} \tag{2}$$

where D_{pi} is the diameter of droplet size class i, ρ_w is the water density, R is the universal gas constant, T is the parcel temperature, p^s is the saturation vapor pressure, D_v is the water vapor diffusivity, M_w is the molar mass of water, ΔH_v is the latent heat of condensation of water, k_a is the thermal conductivity of air, s is the parcel supersaturation, and s_{eq} is the equilibrium supersaturation of the droplet.

Integrating Equation (1) provides the droplet diameter, $D_p(t_{max})$ of an activated CCN at the point of s_{max},

$$D_p^2(t_{max}) = D_p^2(\tau) + 2\int_{\tau}^{t_{max}} G(s - s_{eq})dt \tag{3}$$

where τ is the time at which the CCN activates into a droplet (assumed to occur when the parcel supersaturation is equal to the CCN critical supersaturation, *Nenes and Seinfeld* [2003]), t_{max} is the time in the updraft corresponding to s_{max}, and, $D_p(\tau)$ is the size of CCN at time τ.

Equation (3) can be simplified if droplet growth is assumed to be unaffected by curvature and solute effects (i.e., $s_{eq} = 0$),

$$D_p^2(t_{max}) = D_p^2(\tau) + 2\int_{\tau}^{t_{\max}} Gsdt \tag{4}$$

Since $\int_{\tau}^{t_{\max}} sdt \simeq \frac{1}{2\alpha V}\left[s_{\max}^2 - s(\tau)^2\right]$ [*Twomey*, 1959], substituting into equation (4) gives for $D_p(t_{max})$,

$$D_p(t_{max}) = \sqrt{D_p^2(\tau) + \frac{G}{\alpha V}\left[s_{\max}^2 - s(\tau)^2\right]} \tag{5}$$

For most CCN, $D_p(\tau)$ can be approximated by the critical diameter, $D_c = \frac{2A}{3s_c}$, where $A = \frac{4M_w\sigma_w}{RT\rho_w}$, and M_w, σ_w are the molar mass and surface tension of water, respectively [*Nenes and Seinfeld*, 2003]; $s(\tau)$ can be approximated with the droplet critical supersaturation, $s_c = \frac{4A^3\rho_w M_s}{27\nu\rho_s M_w d_s^3}$, where M_s, ρ_s, ν, are the molar mass, density, effective Van't Hoff factor of the soluble fraction, and d_s is the dry diameter of the CCN from which the droplet formed.

Depending on the particle s_c, *i*) $D_p >> D_c$, *ii*) $D_p << D_c$ (i.e., the CCN never strictly activates), or, *iii*) $D_p \sim D_c$ (i.e., the CCN is very close to the activation point at s_{max}). The particles that have s_c lower than a characteristic "partition supersaturation" [*Nenes and Seinfeld*, 2003; *Fountoukis and Nenes*, 2005; *Barahona and Nenes*, 2007] exhibit behavior type *i* and *ii*, so Equation (5) simplifies to $D_p(t_{\max}) \simeq \sqrt{\frac{G}{\alpha V}\left[s_{\max}^2 - s_c^2\right]}$. The remaining CCN exhibit behavior type *iii*, and $D_p(s_{\max}) \simeq D_c$.

2.2.2. Parcel supersaturation profile beyond s_{max}

The growth of droplets beyond the point of s_{max} in the cloud requires the knowledge of the cloud supersaturation profile. Using the droplet spectrum at s_{max} (section 2.2.1) as an initial condition, we can then compute supersaturation with finite difference over a small time step interval, Δt

$$s(t + \Delta t) = s(t) + \left(\frac{ds}{dt}\right)\Delta t \tag{6}$$

where $s(t)$, $s(t+\Delta t)$ are the supersaturations at time t and $t+\Delta t$, respectively, and ds/dt is the supersaturation tendency in the parcel. Assuming that the droplets are characterized by n size classes with diameters D_{pi}, concentration N_i, and growth rate dD_{pi}/dt (from Equation 1), ds/dt is given by [e.g., *Nenes et al.*, 2001; *Nenes and Seinfeld*, 2003],

$$\frac{ds}{dt} = \alpha V - \gamma \frac{\pi}{2}\frac{\rho_w}{\rho_a}\sum_{i=1}^{n} D_{pi}^2 \frac{dD_{pi}}{dt} N_i \tag{7}$$

where $\alpha = \frac{gM_w\Delta H_v}{c_p RT^2} - \frac{gM_a}{RT}$, $\gamma = \frac{pM_a}{p^s M_w} + \frac{M_w \Delta H_v^2}{c_p RT^2}$, g is the acceleration of gravity, M_a, c_p is the molar mass, heat capacity of air, respectively, and p is the ambient pressure. The first term at the right hand side of Equation (7) represents the availability of water vapor from the

parcel updraft motion (i.e., cooling), and the second term refers to consumption of water vapor by condensation on droplets. All properties in Equation (7) are computed for the average temperature throughout the cloud column, as simulations with a numerical cloud parcel model [*Nenes et al.*, 2001] demonstrate that this assumption does not substantially affect the supersaturation profile over a wide range of cloud conditions. With updated parcel supersaturation (equation 6), the droplets are then grown by integration of equation (1) between time t and $t + \Delta t$,

$$D_{pi}^2(t + \Delta t) = D_{pi}^2(t) + \Delta t \left\{2Gs(t + \Delta t)\right\} \tag{8}$$

The liquid water mixing ratio, W, can be computed as

$$W = \frac{\pi}{6}\frac{\rho_w}{\rho_a}\sum_{i=1}^{n} D_{pi}^3 N_i \tag{9}$$

Equations (6), (8) and (9) can be integrated until the desired liquid water mixing ratio has been reached. If the aerosol size distribution is described in terms of lognormal modes, they are descretized onto size bins that range from $D_{gj} - 10\sigma_j$ to $D_{gj} + 10\sigma_j$, where D_{gj} is the geometric mean diameter of mode j, and σ_j is the geometric standard deviation for mode j.

A series of sensitivity tests were carried out to determine the optimal number of sections used in the parameterization. Using 50 sections per mode and a 0.5 s time step ensured that droplet number calculated with the parameterization agrees with the numerical parcel model predictions to within 5% (not shown).

2.3. Relative dispersion at s_{max} represents the cloud column

In the initial stages of cloud formation, new (small) droplets are continuously formed and grow via condensation. When supersaturation reaches its maximum value, cloud droplet formation ceases, and condensational growth, which exhibits a D_p^{-1} dependency, tends to narrow the distribution over time. This means that within the adiabatic condensational parcel model framework, relative dispersion of the droplet size distribution is largest at the point of maximum supersaturation. If one assumes that relative dispersion at s_{max} is representative of the entire cloud (which implies that the tendency for spectral narrowing from condensation growth is compensated by broadening from entrainment), one can use the approach described in Section 2.2.1 to determine the cloud spectral dispersion.

3. Approaches used to parameterize size distributions

Vertical profiles of droplet distribution characteristics, such as size and relative dispersion, can be computed using either of the three approaches described in Section 2. One issue still remaining however is the treatment of updraft velocity, as droplet distributions can be computed for a single updraft, or a distribution of updrafts. Overall, six approaches are evaluated (summarized in Table 1), as combinations of the droplet growth (Section 2) and updraft distribution treatments (described below), to parameterize droplet size distribution characteristics.

3.1. Single updraft

The droplet distribution computed for a single updraft at a given height (z), $n(D_p, z)$, is used to compute the vertical profile of average droplet diameter, $\overline{D_p}(z)$,

$$\overline{D_p}(z) = \frac{\int_0^\infty D_p n(D_p, z) dD_p}{\int_0^\infty n(D_p, z) dD_p} \tag{10}$$

where $\int_0^\infty n(D_p, z)dD_p = N$ is the total droplet number concentration. The vertical profile of standard deviation, $\sigma(z)$, of the size distribution is given by

$$\sigma(z) = \left(\frac{\int_0^\infty n(D_p, z)(D_p - \overline{D_p}(z))^2 dD_p}{\int_0^\infty n(D_p, z)dD_p} \right)^{1/2} \tag{11}$$

After $\overline{D_p}(z)$ and $\sigma(z)$ are determined, the relative dispersion at any given height, $\varepsilon(z)$ is

$$\varepsilon(z) = \sigma(z)/\overline{D_p}(z) \tag{12}$$

3.2. Distribution of updrafts

Clouds are characterized by a range of updrafts, so that the cumulative droplet size distribution becomes the superposition of distributions from each updraft. Assuming that the updraft distribution can be described with a probability density function (PDF), $p(w)$, the cloud droplet number concentration averaged over $p(w)$ is then computed as

$$N = \int_0^\infty \int_0^\infty p(w)n(D_p, w, z)dD_p dw \tag{13}$$

where by definition $\int_0^\infty p(w)dw = 1$, and, $n(D_p, w, z)$ is the droplet size distribution for a given updraft, w, and height, z. The vertical evolution of average droplet diameter and standard deviation based on averaging a series of updraft runs can be expressed as

$$\overline{D_p}(z) = \frac{\int_0^\infty \int_0^\infty D_p n(D_p, w, z)p(w)dD_p dw}{\int_0^\infty \int_0^\infty p(w)n(D_p, w, z)dD_p dw} \tag{14}$$

$$\sigma(z) = \left(\frac{\int_0^\infty \int_0^\infty n(D_p, w, z)(D_p - \overline{D_p}(z))^2 p(w)dD_p dw}{\int_0^\infty \int_0^\infty p(w)n(D_p, w, z)dD_p dw} \right)^{1/2} \tag{15}$$

227 $\varepsilon(z)$ is computed in a distribution of updrafts with Equation (12). In this study, $p(w)$ is
228 assumed to follow a Gaussian PDF, the moments of which are constrained by the observed
229 average and standard deviation of updraft velocity.

4. Evaluating droplet growth approaches

230 Each droplet approach is evaluated using in-situ measurements of ambient cloud droplet
231 size distributions collected during the CRYSTAL-FACE and CSTRIPE field campaigns
232 [*Conant et al.*, 2004; *Meskhidze et al.*, 2005]. Simulations were carried out for the aerosol
233 characteristics summarized in Table 2 for CRYSTAL-FACE, and Table 3 for CSTRIPE
234 data. *Hsieh et al.* [in press] give a description of the cloud conditions, instrumentation and
235 cloud droplet distribution characteristics for both datasets. To ensure that the observed
236 distributions used to evaluate each approach were not influenced by the effects of collision-
237 coalescence, we select horizontal transects for which the droplet distributions are single-
238 mode and the liquid water content is within a factor of two of the adiabatic value. All of
239 the CSTRIPE data fit this criterion, while the subset of CRYSTAL-FACE dataset used
240 is summarized in Table 4.

241 In the sections that follow, we first evaluate the parameterization against the parcel
242 model for cloud data measured during CRYSTAL-FACE and CSTRIPE. The predictions
243 are then evaluated against the in-situ data; spectral quantities are compared at the cloud
244 height where predicted LWC is equal to the measured value. Given that the ability of
245 each approach to reproduce droplet number was evaluated by *Conant et al.* [2004] and
246 *Meskhidze et al.* [2005], this study focuses primarily on spectral dispersion.

4.1. Comparison of parcel model and parameterization

The parameterized parcel model is first evaluated by comparing predicted droplet mean size, spectrum width, and relative dispersion against those of a full numerical activation adiabatic parcel model [*Nenes et al.*, 2001]. Based on the suggestion of *Fountoukis et al.* [2007], we use an effective water vapor uptake coefficient, α, of 0.06. Figure 2 shows the predicted relative dispersion from parameterization (PS approach) and parcel model (MS approach) for all clouds sampled. The comparison is carried out at the observed LWC. $\overline{D_p}$ is always well captured, as the discrepancy between parameterization and parcel model rarely exceeds 5% (Figure 1). Parameterized relative dispersion agrees with the parcel model, for most cases, to within 30% (Figure 2). The reasonably good agreement between numerical and parameterized parcel model suggests that the latter can be used for predictions of cloud droplet distributions in place of the full parcel model.

4.2. Comparison against observations

Predicted droplet spectra using the MS, PS approaches agree reasonably with observations for transect 4 (T4) when the cloud droplet size distributions are narrow, liquid water content is close to the adiabatic values, and the distribution is measured close to cloud base. An example of such a situation is given in Figure 3; uncertainties in measured cloud base are likely responsible for the shift between observed and measured distributions. Spectral broadening can also occur from instrument artifacts, such as laser beam non-homogeneity and coincidence error. *Wendisch et al.* [1996] demonstrated that beam non-homogeneity in the FSSP overestimates droplet size by 10-15% when in the 15-30 micron size range, and, by 5-10% for 30-50 micron droplets. However, the same study indicated that spectrum broadening is negligible between 2 and 14 micron radius

(which covers the majority of observed distributions in CSTRIPE and CRYSTAL-FACE). *Wendisch et al.* [1996] and *Baumgardner and Spowart* [1990] indicated that instrument response time may cause broadening of the distribution for air speeds higher than 55-60 m s^{-1}. Given that the Twin Otter platform operational velocity ranges between 50 - 55 m s^{-1}, broadening due to air speed is negligible. Coincidence error can also lead to broadening of the distribution when CDNC > 500 cm^{-3} *Brenguier* [1998]. Using this criterion, only a small fraction of the data could be affected, as the 75^{th} percentile of CSTRIPE data has CDNC below 370 cm^{-3}, and CRYSTAL-FACE, below 590 cm^{-3}.

Most often, however, predictions deviate significantly from observations, and is not a result of measurement uncertainty. This is shown in Figure 4, which shows the predicted relative dispersion for all six approaches versus measured values for CRYSTAL-FACE and CSTRIPE distributions. The predicted values from the parameterized parcel model are close to the results based on the numerical parcel model; however, the MS, PS approaches tend to predict narrow distributions relative to those measured. On average, relative dispersion was substantially underestimated by both numerical and parameterized parcel models using single updrafts (MS, PS). Integrating over updraft distributions (MP, PP) tends to increase predicted relative dispersion, although relative dispersion is still underestimated on average by a factor of two (Table 5). SS and SP approaches agree more closely with measurements, suggesting that when considering only condensational growth, the relative dispersion at s_{max} is a better representation of the cloud droplet size distribution than a full treatment with a 1D parcel model. This implies, to first order, that spectral narrowing from condensation balances broadening from entrainment and mixing processes. Substantial efforts have been made to sample cloud data with positive

vertical velocity; nevertheless, a small fraction of downdrafts (especially for the weaker updrafts in CSTRIPE clouds) may exist in the dataset, and contribute to the discrepancy between observed and predicted spectral dispersion.

4.3. Sensitivity of relative dispersion to the effective water uptake coefficient

It is important to assess the sensitivity of predicted spectral dispersion on the water vapor uptake coefficient, α, as the latter is a highly uncertain parameter [*Kanakidou et al.*, 2005; *Ruehl et al.*, 2007] that can have a profound impact on droplet number and size. This sensitivity exercise is shown in Figure 5, where predicted spectral dispersion (using the SP approach; Table 1) is presented against observations. The range of α considered (0.03 to 1.0) is based on the suggestions of *Fountoukis et al.* [2007], whom found that this range gives CDNC closure to within measurement uncertainty for clouds sampled during the ICARTT campaign. Overall, the water uptake coefficient has a minimal impact on relative dispersion since the normalized mean error in ε is -5.2 $\pm$ 33.8 %(0.1 $\pm$ 28.3 %) for CRYSTAL-FACE (CSTRIPE) and $\alpha = 1$, -10.4 $\pm$ 32.1 % (-0.7 $\pm$ 26.1 %) when $\alpha =$ 0.06, and, -14.4 $\pm$ 31.6 % (-2.9 $\pm$ 25.4 %) for $\alpha = 0.03$.

4.4. Relationship between relative dispersion and droplet number concentration

Liu et al. [2006] show an increase in aerosol loading (with everything else constant) leads to a positive correlation between dispersion and droplet concentration. An increase, however, in updraft leads to a negative correlation between dispersion and droplet concentration. We attempt to explore which effects (aerosol number or dynamics) dominate the spectral dispersion in the data of our study. Figure 6 presents observed and predicted spectral dispersion versus droplet number for all analyzed clouds from (a) CRYSTAL-

311 FACE and (b) CSTRIPE. A negative correlation is found between spectral dispersion
312 and droplet number. This implies that, in terms of the dispersion-droplet concentration
313 relationship, the dynamical variation in the analyzed data is stronger than the variation
314 from aerosol loading.

4.5. Prediction of k

315 The six approaches are evaluated in terms of their ability to reproduce the spectral shape
316 parameter k, which is the cube of the ratio of volumetric to effective radius (the analysis
317 could also be done instead terms of the more mathematically consistent β parameter of *Liu*
318 *and Daum* [2004], defined as r_e over the droplet volumetric radius; both analysis however
319 are equivalent). Figure 7 shows the comparison of k between the predictions and measured
320 data. k is substantially overpredicted using the MS, MP, PS and PP approaches for the
321 majority of the data considered, consistent with the fact that these approaches predict
322 narrow droplet distributions relative to those measured. Compared to CRYSTAL-FACE
323 data, k is further overestimated in the CSTRIPE data (Figure 7, Table 5), consistent
324 with the complex dynamics in stratocumulus clouds. With the exception of SS and SP
325 approaches, deviations in predicted k (Table 5) is too large, being comparable to the range
326 seen for k in the whole cloud dataset. The scatter in predicted k is fairly large, even for
327 SS, SP; whether it is important for indirect forcing assessments requires the application
328 of a global model, and is left for a future study.

4.6. Prediction of autoconversion

We now address the uncertainty in autoconversion that results from discrepancy in predicted spectral dispersion associated with each approach of Table 1. For this purpose,

the R_6 autoconversion parameterization of *Liu and Daum* [2004] is used,

$$P_6 = \alpha_6 N^{-1/3} L^{7/3} H\left(R_6 - R_{6c}\right) \tag{16}$$

where P_6 is the autoconversion rate. N is the cloud drop number concentration, L is the liquid water content. H stands for the Heaviside function which characterizes the threshold process that controls the onset of autoconversion as the sixth moment of the cloud drop distribution, R_6, is greater than the specified threshold value R_{6c}. Finally, $\alpha_6 = \left(\frac{3}{4\pi\rho_w}\right)^2 k_2 \beta_6^6 \left(\frac{L}{N}\right)^{2/3}$, where $k_2 = 1.9 \times 10^{11}$ cm^{-3}s^{-1} and β_6 is a parameter related to the relative dispersion of a gamma distribution,

$$\beta_6 = \left[\frac{\left(1+3\varepsilon^2\right)\left(1+4\varepsilon^2\right)\left(1+5\varepsilon^2\right)}{\left(1+\varepsilon^2\right)\left(1+2\varepsilon^2\right)}\right]^{1/6} \tag{17}$$

The R_6 parameterization is used for two reasons: *i*) it predicts the total coalescence rate and gives an upper limit for autoconversion (and discrepancy thereof), [*Hsieh et al.*, in press; *Wood*, 2005], and, *ii*) total coalescence computed from the kinetic collection equation is in good agreement with R_6 for the data considered in this study [*Hsieh et al.*, in press]. Autoconversion calculations are done only for CRYSTAL-FACE clouds, given that CSTRIPE clouds are far from a precipitating state [*Hsieh et al.*, in press].

Figure 8 shows the R_6 predicted autoconversion rate, calculated based on approaches in Table 1 compared to that computed from measured cloud spectra. A summary of the normalized mean error and standard deviation is given in Table 5. Because the predicted autoconversion rates are computed using the same liquid water content as the measured values, the discrepancy between the prediction and the measurement is due to the difference in cloud droplet number and relative dispersion. On average, MS, MP, PS, PP

underestimate R_6 autoconversion rate for CRYSTAL-FACE and CSTRIPE clouds on average by a factor of 3, mostly because of their underestimation of droplet relative dispersion. The autoconversion discrepancy can be large as a factor of 10, which is larger than the inherent variability of the parameterization [*Hsieh et al.*, in press]. The SS, SP tend to be in better agreement with autoconversion rate predicted from the observed spectra (Figure 8) and tends to be within the estimated uncertainty of the parameterization.

5. Summary

This work examines the ability of physically-based 1-D adiabatic parcel approaches to parameterize the cloud droplet distribution characteristics relevant for computation of cloud effective radius and autoconversion in regional/global atmospheric models. A total of six approaches is examined, which are combinations of a numerical parcel model, a simplified parameterization, and their integrations over single updrafts and distributions thereof. Integrations are applied assuming that *i*) conditions at s_{max} are reflective of the cloud column, or, *ii*) cloud properties vary vertically, in agreement with 1-D parcel theory. Good agreement of droplet relative dispersion between parcel model frameworks indicates the parameterized parcel model captures most of the 1-D dynamics of the numerical model. When compared against in-situ cloud droplet observations obtained during the CRYSTAL-FACE and CSTRIPE missions, the distributions predicted with the parcel model (for single updrafts and distributions thereof) are too narrow, with relative dispersion being on average a factor of 2 lower than observations. However, if conditions at cloud maximum supersaturation are used to predict relative dispersion and applied throughout the cloud column, a better agreement is seen with observations, especially if integrations are done over the relevant distribution of updraft velocity; this implies that spectral nar-

rowing from condensational growth is largely balanced by broadening from entrainment. The superiority of the latter method is reflected in predictions of the spectral dispersion parameter k (used for calculation of effective radius), but to a lesser degree in calculations of autoconversion; nevertheless, the simplicity of calculating spectral dispersion at s_{max} is attractive. Evaluation of this method however with additional in-situ cloud datasets is required before it could be recommended for usage in large scale models.

Although the SS, SP methods outperformed all approaches considered, they are based on adiabatic cloud parcel theory and may still introduce unacceptable levels of uncertainty in global modeling. Given that clouds are diabatic, parameterization that accounts for some degree of entrainment (e.g., *Barahona and Nenes* [2007]) may address this issue and further improve predictions. Such an application will be the subject of future work.

Acknowledgments. This research was funded by the Department of Energy, an NSF CAREER award, a NASA New Investigator Award, and a graduate teaching assistantship from the School of Earth and Atmospheric Science at Georgia Institute of Technology. This work was also funded by the office of Naval Research under grant N00014-04-1-0118. We also thank three anonymous reviewers for comments that improved the paper.

References

Abdul-Razzak, H., S. J. Ghan, and C. Rivera-Carpio, A parameterization of aerosol activation: 1. single aerosol type, *J. Geophys. Res.*, *103*, 6123–6132, 1998.

Albrecht, B. A., Aerosols, cloud microphysics, and fractional cloudiness, *Science*, *245*, 1227–1230, 1989.

389 Baker, M. B., R. G. Corbin, and J. Latham, The influence of entrainment on the evolution
390 of cloud droplet spectra: I. A model of inhomogeneous mixing, *Quart. J. R. Met. Soc.*,
391 *106*, 581–598, 1980.

392 Barahona, D., and A. Nenes, Parameterization of cloud droplet formation in
393 large scale models: including effects of entrainment, *J. Geophys. Res.*, *110*,
394 doi:10.1029/2007JD008,473, 2007.

395 Baumgardner, D., and M. Spowart, Evaluation of the Foward Scattering Spectrometer
396 Probe. part III: Time response and laser inhomogeneity limitations, *J. Atmos. Ocean.*
397 *Tech.*, *7*, 666–672, 1990.

398 Boucher, O., and U. Lohmann, The sulfate-ccn-cloud albedo effect: A sensitivity study
399 with 2 general-circulation models, *Tellus*, *47*, 281–300, 1995.

400 Brenguier, T. B. A. D. C. J. I. R. P. D. T. . P. W., J. L., Improvements of droplet
401 size distribution measurements with the Fast-FSSP (Forward Scattering Spectrometer
402 Probe), *J. Atmos. Ocean. Tech.*, *15*, 1077–1090, 1998.

403 Conant, W., T. Vanreken, T. Rissman, V. Varutbangkul, J. Jimenez, A. Delia,
404 R. Bahreini, G. Roberts, A. Nenes, H. Jonsson, R. C. Flagan, and J. H. Seinfeld,
405 Aerosol-cloud drop concentration closure in warm cumulus, *J. Geophys. Res.*, *109*,
406 D13,204, doi:10.1029/2003JD004,324, 2004.

407 Cooper, W. A., Effects of variable droplet growth histories on droplet size distributions.
408 Part I: Theory, *J. Atmos. Sci.*, *46*, 1301–1311, 1989.

409 Erlick, C., A. Khain, M. Pinsky, and Y. Segal, The effect of wind velocity fluctuations on
410 drop spectrum broadening in stratocumulus clouds, *Atmos. Res.*, *75*, 15–45, 2005.

411 Fountoukis, C., and A. Nenes, Continued development of a cloud droplet for-
412 mation parameterization for global climate models, *J. Geophys. Res.*, *110*,
413 doi:10.1029/2004JD005,591, 2005.

414 Fountoukis, C., A. Nenes, N. Meskhidze, R. Bahreini, W. C. Conant, H. Jonsson, S. Mur-
415 phy, A. Sorooshian, V. Varutbangkul, F. Brechtel, R. C. Flagan, and J. H. Seinfeld,
416 Aerosol-cloud drop concentration closure for clouds sampled during the international
417 consortium for atmospheric research on transport and transformation 2004 campaign,
418 *J. Geophys. Res.*, *112*, doi:10.1029/2006JD007,272, 2007.

419 Ghan, S. J., L. R. Leung, and R. C. Easter, Prediction of cloud droplet number in a
420 general circulation model, *J. Geophys. Res.*, *102 (D18)*, 21,777–21,794, 1997.

421 Hsieh, W. C., H. Jonsson, G. Buzorius, R. C. Flagan, J. H. Seinfeld, and A. Nenes, On
422 the representation of droplet coalescence and autoconversion: Evaluation using ambient
423 cloud droplet size distributions, *J. Geophys. Res.*, in press.

424 Intergovernmental Panel on Climate Change (IPCC), *Climate Change 2007: The Physical*
425 *Science Basis*, Cambridge University Press, UK, 2007.

426 Kanakidou, M., J. H. Seinfeld, S. N. Pandis, I. Barnes, F. J. Dentener, M. C. Facchini,
427 R. Van Dingenen, B. Ervens, A. Nenes, C. J. Nielsen, E. Swietlicki, J. P. Putaud,
428 Y. Balkanski, S. Fuzzi, J. Horth, G. K. Moortgat, R. Winterhalter, C. E. L. Myhre,
429 K. Tsigaridis, E. Vignati, E. G. Stephanou, and J. Wilson, Organic aerosol and global
430 climate modelling: a review, *Atmos. Chem. Phys.*, *5*, 1053–1123, 2005.

431 Kessler, E., On the distribution and continuity of water substance in atmospheric circu-
432 lation, *Tech. Rep. 32*, Meteor. Monogr., Amer. Meteor. Soc., 1969.

433 Khairoutdinov, M., and Y. Kogan, A new cloud physics parameterization in a large-eddy
434 simulation model of marine stratocumulus, *Mon. Wea. Rev.*, *128*, 229–243, 2000.
435 Khvorostyanov, V., and J. Curry, Toward the theory of stochastic condensation in clouds.
436 part II: Analytical solutions of the gamma-distribution type., *J. Aerosol Sci.*, *56*, 3997–
437 4013, 1999.
438 Lasher-Trapp, S. G., W. A. Cooper, and A. M. Blyth, Broadening of droplet size distri-
439 butions from entrainment and mixing in a cumulus cloud, *Quart. J. R. Met. Soc.*, pp.
440 195–220, 2005.
441 Liu, Y., and P. H. Daum, Spectral dispersion of cloud droplet size distributions and the
442 parameterization of cloud droplet effective radius, *Geophys. Res. Lett.*, *27 (13)*, 1903–
443 1906, 2000.
444 Liu, Y., and P. H. Daum, Indirect warming effect from dispersion forcing, *Nature*, *419*,
445 580–581, 2002.
446 Liu, Y., and P. H. Daum, Parameterization of the autoconversion process. part i : Analyt-
447 ical formulation of the kessler-type parameterizations, *J. Atmos. Sci.*, *61*, 1539–1548,
448 2004.
449 Liu, Y., P. H. Daum, and S. S. Yum, Analytical expression for the relative dispersion of
450 the cloud droplet size distribution, *Geophys. Res. Lett.*, *33*, doi:10.1029/2005GL024,052,
451 2006.
452 Lohmann, U., and J. Feichter, Global indirect aerosol effects: a review, *Atmos. Chem.*
453 *Phys.*, *5*, 715–737, 2005.
454 Manton, M. J., and W. R. Cotton, Formulation of approximate equations for modeling
455 moist deep convection on the mesoscale, Ph.D. thesis, Colorado State University, 1977.

Martin, G. M., D. W. Johnson, and A. Spice, The measurement and parameterization of effective radius of droplets in warm stratocumulus clouds, *J. Atmos. Sci.*, *51*, 1823–1842, 1994.

Mason, B. J., and C. W. Chien, Cloud-droplet growth by condensation in cumulus, *Quart. J. R. Met. Soc.*, *88*, 136–142, 1962.

Mason, B. J., and P. R. Jonas, The evolution of droplet spectra and large droplets by condensation in cumulus clouds, *Quart. J. R. Met. Soc.*, *100*, 23–38, 1974.

Meskhidze, N., A. Nenes, W. C. Conant, and J. H. Seinfeld, Evaluation of a new cloud droplet activation parameterization with in situ data from CRYSTAL-FACE and CSTRIPE, *J. Geophys. Res.*, *110*, doi:10.1029/2004JD005,703, 2005.

Nenes, A., and J. H. Seinfeld, Parameterization of cloud droplet formation in global climate models, *J. Geophys. Res.*, *108*, doi:10.1029/2002JD002,911, 2003.

Nenes, A., S. Ghan, H. Abdul-Razzak, P. Chuang, and J. Seinfeld, Kinetic limitations on cloud droplet formation and impact on cloud albedo, *Tellus*, *53*, 133–149, 2001.

Peng, Y., and U. Lohmann, Sensitivity study of the spectral dispersion of the cloud droplet size distribution on the indirect aerosol effect, *Geophys. Res. Lett.*, *30*, doi:10.1029/2003GL017,192, 2003.

Peng, Y., U. Lohmann, and R. Leaitch, Importance of vertical velocity variations in the cloud droplet nucleation process of marine stratus clouds, *J. Geophys. Res.*, *110*, doi:10.1029/2004JD004,922, 2005.

Peng, Y., U. Lohmann, R. Leaitch, and M. Kulmala, An investigation into the aerosol dispersion effect through the activation process in marine stratus clouds, *J. Geophys. Res.*, *112*, doi:10.1029/2006JD007,401, 2007.

Pruppacher, H. R., and J. D. Klett, *Microphysics of Clouds and Precipitation*, Kluwer Acad., Norwell, Mass., 1997.

Rotstayn, L., and Y. Liu, Sensitivity of the first indirect aerosol effect to an increase of cloud droplet spectral dispersion with droplet number concentration, *J. Climate*, *16*, 3476–3481, 2003.

Rotstayn, L. D., A physically based scheme for the treatment of stratiform clouds and precipitation in large-scale models: I: Description and evaluation of the microphysical processes, *Q.J.R. Meteorol. Soc.*, *123*, 1227–1282, 1997.

Ruehl, C. R., A. Nenes, and P. Y. Chuang, How quickly do cloud droplets form on atmospheric particles?,, *Atmos. Chem. Phys. Discuss.*, *7*, 14,233–14,264, 2007.

Seinfeld, J., and S. Pandis, *Atmospheric chemistry and physics: from air pollution to climate change*, John Wiley, New York, 1998.

Su, C. W., S. K. Krueger, P. A. McMurtry, and P. H. Austin, Linear eddy modeling of droplet spectral evolution during entrainment and mixing in cumulus clouds, *Atmos. Res.*, *47-48*, 41–58, 1998.

Twomey, S., The nuclei of natural cloud formation. II. The supersaturation in natural clouds and the variation of cloud droplet concentration, *Geofisica Pura Appl.*, *43*, 243–249, 1959.

Twomey, S., The influence of pollution on the shortwave albedo of clouds, *J. Atmos. Sci.*, *34*, 1149–1152, 1977.

Wendisch, M., A. Keil, and A. V. Korolev, FSSP characterization with monodisperse water droplets, *J. Atmos. Ocean. Tech.*, *13*, 1152–1165, 1996.

Wood, R., Drizzle in stratiform boundary layer clouds. part II: Microphysical aspects., *62*, 3034–3050, 2005.

Yum, S. S., and J. G. Hudson, Adiabatic predictions and observations of cloud droplet spectral broadness, *Atmos. Res.*, *73*, 203–223, 2005.

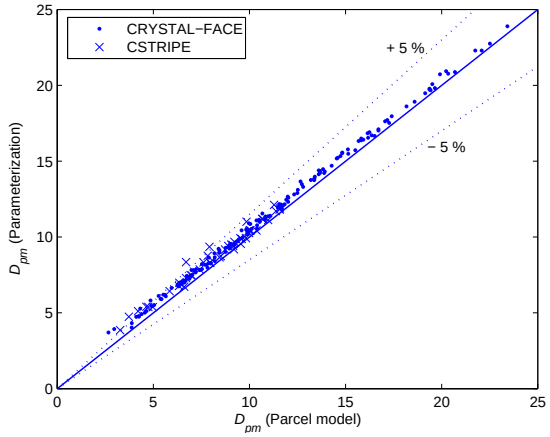

Figure 1. Mean droplet diameter (μm) as predicted by numerical and parameterized parcel models (MS, PS approaches) based on aerosol characteristics measured during CRYSTAL-FACE and CSTRIPE.

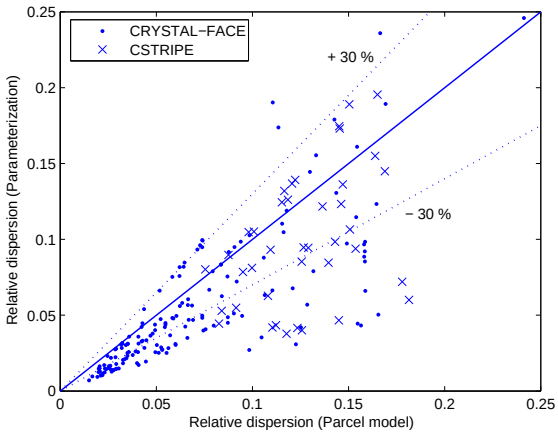

Figure 2. Same as Figure 1 but for prediction of relative dispersion.

Table 1. Approaches used to parameterize droplet size distribution characteristics.

Symbol	Description of approach
MS	Numerical parcel model, single updraft. $\overline{D_p}(z)$, $\sigma(z)$, and $\varepsilon(z)$ computed as described in Sections 2.1, 3.1
MP	Numerical parcel model, distribution of updrafts. $\overline{D_p}(z)$, $\sigma(z)$, and $\varepsilon(z)$ computed as described in Sections 2.1, 3.2
PS	Parameterized parcel model, single updraft. $\overline{D_p}(z)$, $\sigma(z)$, and $\varepsilon(z)$ computed as described in Sections 2.2, 3.1
PP	Parameterized parcel model, distribution of updrafts. $\overline{D_p}(z)$, $\sigma(z)$, and $\varepsilon(z)$ computed as described in Sections 2.2,3.2
SS	$\varepsilon(z)$ at s_{max} for a single updraft apply to the whole cloud column. Parameterized parcel model used.
SP	$\varepsilon(z)$ at s_{max} for a distribution of updrafts apply to the whole cloud column. Parameterized parcel model used.

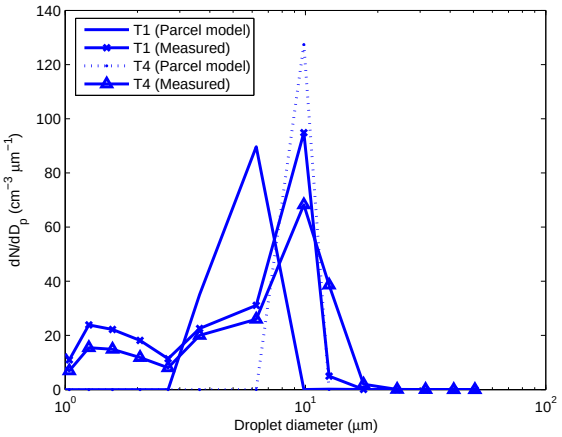

Figure 3. Observed and predicted (using approach PS) droplet spectra for CRYSTAL-FACE cloud C12-1. T1 and T4 refer to transect 1 and 4 of C12-1 [*Meskhidze et al.*, 2005]

.

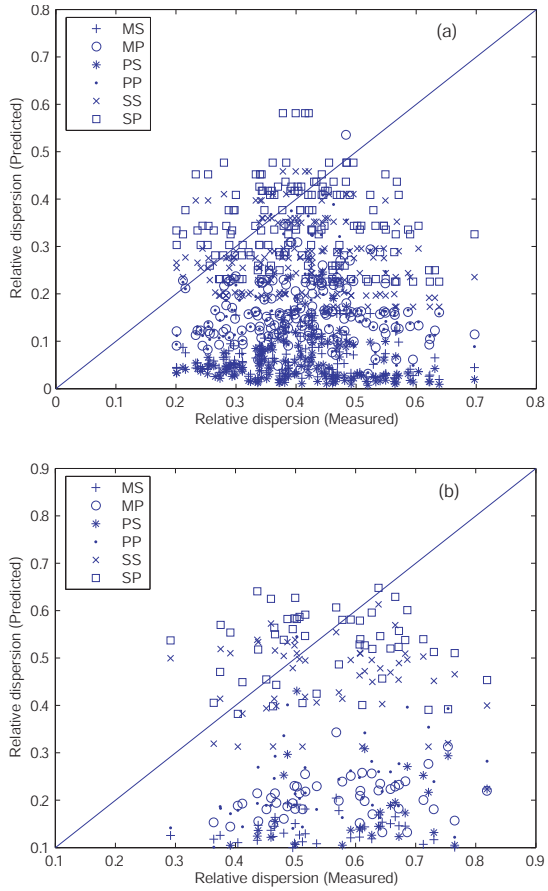

Figure 4. Prediction of relative dispersion by six approaches summarized in Table 1 compared to measurement for clouds sampled during (a) CRYSTAL-FACE and (b) CSTRIPE.

Table 2. Characteristics of aerosol sampled during CRYSTAL-FACE. Size distribution is composed of four lognormal modes, with modal diameter, D_{pgi} in μm, geometric standard deviation, σ_i in μm, and concentration, N_i in cm^{-3}. Flight naming adopted from *Meskhidze et al.* [2005].

Flight	D_{pg1}	σ_1	N_1	D_{pg2}	σ_2	N_2	D_{pg3}	σ_3	N_3	D_{pg4}	σ_4	N_4
H4-1	0.011	1.32	321.8	0.052	1.49	296.8	0.15	1.45	190.3	-	-	-
H4-2	0.012	1.35	174.7	0.064	1.83	635.8	0.49	1.23	5.3	-	-	-
H4-3	0.022	1.15	15.1	0.051	1.46	215.5	0.14	1.50	168.9	-	-	-
C4	0.019	1.31	179.4	0.049	1.44	817.7	0.12	1.53	493.0	1.55	1.30	0.5
C6-1	0.012	1.13	21.1	0.038	1.60	287.8	0.13	1.41	117.0	1.66	1.22	2.7
C6-2	0.016	1.19	31.6	0.039	1.53	280.0	0.11	1.39	117.0	1.50	1.31	0.3
C6-3	0.014	1.25	97.6	0.047	1.63	672.8	0.13	1.42	187.3	1.60	1.28	0.3
C8-1	0.019	1.31	21.9	0.104	1.99	1246.0	0.61	1.25	6.2	1.62	1.27	1.5
C8-2	0.014	1.22	68.7	0.114	2.02	1127.0	0.52	1.21	11.6	1.56	1.30	1.6
C10-1	0.015	1.40	459.2	0.035	1.24	421.8	0.11	1.71	3325.0	1.57	1.30	0.5
C10-2	0.011	1.07	47.3	0.033	1.65	3833.0	0.11	1.64	3162.0	1.52	1.30	0.6
C11-1	0.020	1.10	27.6	0.095	2.06	2143.0	0.57	1.25	3.5	1.63	1.27	0.5
C11-2	0.014	1.20	181.7	0.037	1.61	1369.0	0.12	1.78	2493.0	1.77	1.20	2.1
C12-1	0.010	1.08	16.8	0.045	1.44	211.0	0.14	1.57	270.4	1.59	1.29	0.4
C12-2	0.011	1.21	137.9	0.056	1.59	241.4	0.15	1.43	259.8	1.58	1.29	0.8
C16-1	0.013	1.10	37.3	0.031	1.57	355.3	0.12	1.52	133.8	1.51	1.31	0.4
C16-2	0.017	1.26	84.1	0.033	1.54	305.6	0.14	1.35	117.6	1.65	1.25	0.6
C17-1	0.012	1.11	67.6	0.024	1.53	803.4	0.15	1.53	235.6	1.67	1.22	1.5
C17-2	0.011	1.06	51.4	0.021	1.70	494.8	0.15	1.54	226.1	1.63	1.19	1.4
C17-3	0.011	1.05	47.4	0.025	1.79	829.0	0.14	1.61	290.0	1.74	1.21	3.5

Table 3. Same as Table 2, but for aerosol sampled during CSTRIPE.

Flight	D_{pg1}	σ_1	N_1	D_{pg2}	σ_2	N_2	D_{pg3}	σ_3	N_3	D_{pg4}	σ_4	N_4
CS1	0.012	1.08	29.3	0.059	1.55	1550.0	0.18	1.31	323.7	0.54	1.21	8.6
CS2	0.013	1.19	4.2	0.061	1.32	263.7	0.16	1.53	338.0	0.83	1.06	1.0
CS3	0.029	1.18	15.6	0.064	1.47	1361.0	0.92	1.18	7.0	1.42	1.27	21.7
CS4	0.011	1.03	1.1	0.058	1.40	617.5	0.15	1.46	366.4	0.53	1.44	8.6
CS5	0.014	1.04	2.9	0.060	1.47	871.7	0.15	1.42	362.5	0.66	1.14	6.8
CS6	0.013	1.06	2.2	0.055	1.39	256.4	0.16	1.55	219.4	0.70	1.21	3.0
CS7	0.011	1.03	1.4	0.064	1.43	481.8	0.15	1.44	393.7	1.55	1.25	0.3
CS8	0.014	1.04	1.4	0.095	1.95	650.3	0.58	1.05	1.2	0.72	1.13	0.4

Table 4. Observed and modeled D_{pavg} (μm), σ (μm), ε for CRYSTAL-FACE clouds used in this study. Predictions carried out with the MS approach.

Flight (cloud)	D_{pavg} obs (pred)	σ obs (pred)	ε obs (pred)
C6 (1- 1)	12.48 (11.73)	3.93 (1.45)	0.31 (0.12)
C6 (3- 2)	9.47 (6.93)	1.80 (1.43)	0.19 (0.21)
C8 (1- 1)	4.34 (4.69)	1.78 (1.45)	0.41 (0.31)
C8 (1- 2)	4.70 (5.17)	1.91 (1.40)	0.41 (0.27)
C10 (1-10)	8.57 (6.54)	1.99 (0.99)	0.23 (0.15)
C12 (1- 1)	8.47 (5.98)	2.19 (0.82)	0.26 (0.14)
C12 (1- 2)	9.58 (8.08)	2.42 (1.81)	0.25 (0.22)
C12 (1- 3)	8.53 (8.08)	2.27 (1.81)	0.27 (0.22)
C12 (1- 4)	9.43 (9.85)	2.88 (0.24)	0.31 (0.02)
C12 (1- 5)	14.47 (13.27)	3.15 (1.75)	0.22 (0.13)
C12 (2- 2)	8.31 (9.50)	2.04 (1.12)	0.25 (0.12)
C16 (2- 2)	13.25 (11.99)	3.43 (1.13)	0.26 (0.09)
C16 (2- 3)	14.86 (15.03)	3.94 (2.46)	0.27 (0.16)
C17 (1- 1)	9.53 (11.69)	2.70 (1.32)	0.28 (0.11)
C17 (1- 2)	13.66 (14.12)	3.24 (2.31)	0.24 (0.16)
C17 (2- 4)	11.07 (9.97)	3.25 (0.73)	0.29 (0.07)
C17 (2- 5)	13.95 (17.45)	5.13 (0.31)	0.37 (0.02)
C17 (3- 2)	11.49 (11.46)	2.33 (1.43)	0.20 (0.12)
H4 (1- 1)	9.27 (9.10)	3.22 (1.46)	0.35 (0.16)
H4 (2- 2)	8.63 (9.65)	1.87 (0.93)	0.22 (0.10)
H4 (2- 3)	8.98 (9.93)	1.89 (0.50)	0.21 (0.05)
H4 (3- 2)	10.18 (10.57)	1.93 (1.20)	0.19 (0.11)
H4 (3- 3)	9.61 (9.88)	1.91 (0.34)	0.20 (0.03)

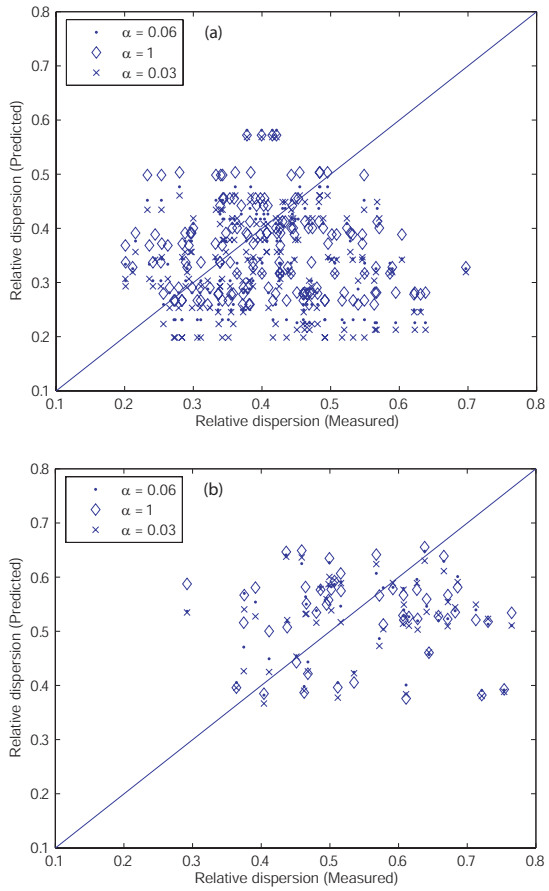

Figure 5. Predicted versus measured relative dispersion (SP approach) for a range of α for (a) CRYSTAL-FACE, and, (b) CSTRIPE clouds.

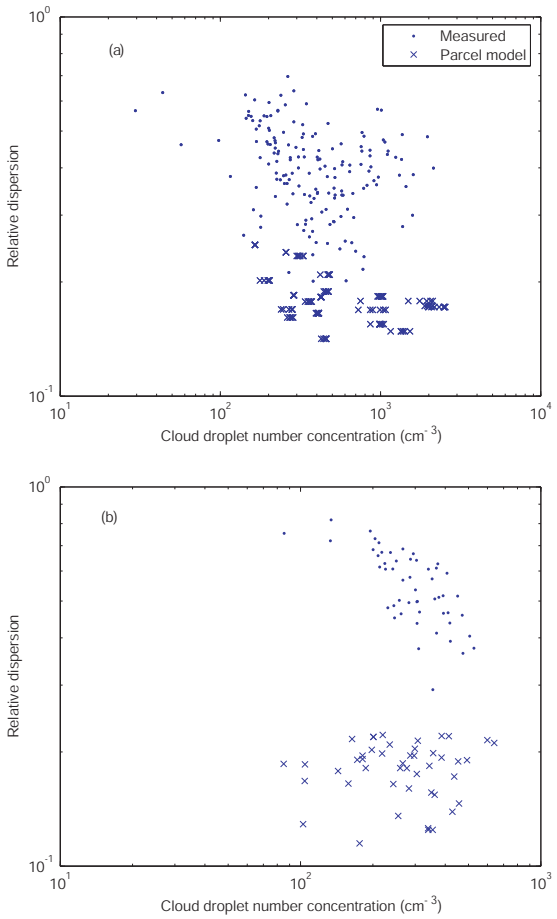

Figure 6. Measured and predicted relative dispersion versus droplet number concentration for (a) CRYSTAL-FACE, and, (b)CSTRIPE clouds. The predicted data is based on droplet size distributions at s_{max} for single updraft velocity from parcel model simulations.

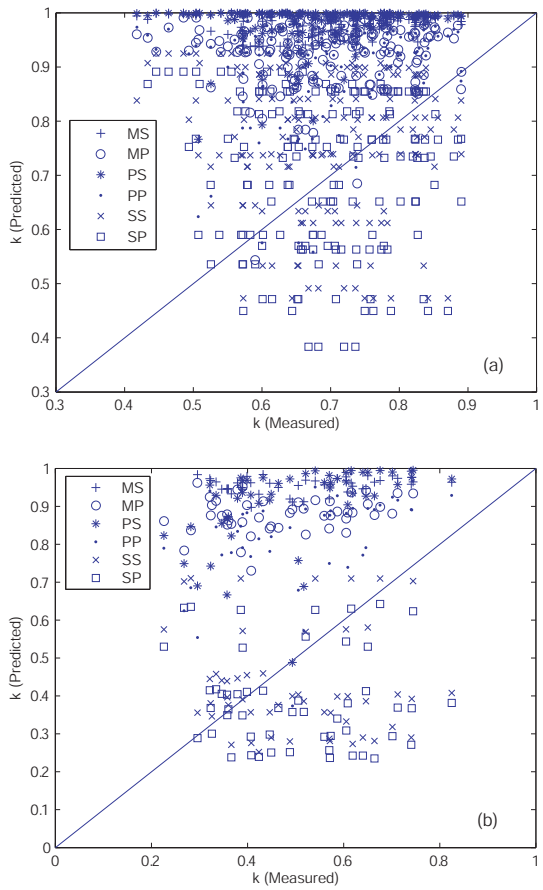

Figure 7. Observed vs. predicted k using the six approaches of Table 1 for (a) CRYSTAL-FACE, and, (b) CSTRIPE clouds.

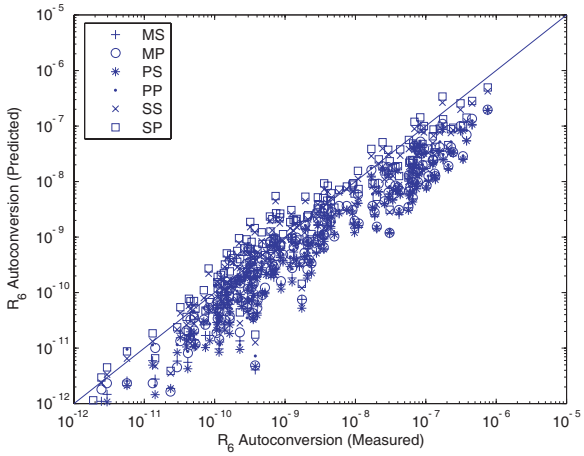

Figure 8. Observed vs. predicted autoconversion rate [kg m^{-3} s^{-1}] using the six approaches of Table 1 for CRYSTAL-FACE clouds.

Table 5. Normalized (%) mean fractional error (standard deviation) of predicted ε, k and autoconversion rate for the CRYSTAL-FACE and CSTRIPE droplet distributions.

Data set	Approach	relative dispersion	k	P_6 autoconversion
CRYSTAL-FACE	MS	-85.37(32.25)	41.30(44.27)	-66.38(24.63)
CRYSTAL-FACE	MP	-58.92(19.04)	37.04(25.20)	-58.24(32.99)
CRYSTAL-FACE	PS	-87.42(25.32)	43.37(35.53)	-68.09(24.19)
CRYSTAL-FACE	PP	-55.67(21.64)	34.12(25.30)	-59.45(31.48)
CRYSTAL-FACE	SS	-28.51(27.19)	13.79(29.61)	97.26(1278.90)
CRYSTAL-FACE	SP	-10.41(32.09)	4.97(29.62)	181.70(2011.80)
CSTRIPE	MS	-91.51(51.80)	46.84(170.20)	-
CSTRIPE	MP	-62.77(8.29)	99.46(59.90)	-
CSTRIPE	PS	-83.90(40.35)	76.89(106.70)	-
CSTRIPE	PP	-56.73(16.27)	74.22(53.38)	-
CSTRIPE	SS	-13.19(24.82)	-3.50(51.24)	-
CSTRIPE	SP	- 0.71(26.07)	-12.72(46.61)	-